BSA-Mediated Synthesis of Bismuth Sulfide Nanotheranostic Agents for Tumor Multimodal Imaging and Thermoradiotherapy

Yong Wang, Yongyou Wu, Yujing Liu, Jia Shen, Ling Lv, Liubing Li, Liecheng Yang, Jianfeng Zeng, Yangyun Wang, Leshuai W. Zhang, Zhen Li,* Mingyuan Gao,* and Zhifang Chai*

Fabrication of ultrasmall single-component omnipotent nanotheranostic agents integrated with multimodal imaging and multiple therapeutic functions becomes more and more practically relevant but challenging. In this article, sub 10 nm Bi_2S_3 biocompatible particles are prepared through a bovine serum albumin (BSA)-mediated biomineralization process under ambient aqueous conditions. Owing to the ultrasmall size and colloidal stability, the resulting nanoparticles (NPs) present outstanding blood circulation behavior and excellent tumor targeting ability. Toward theranostic applications, the biosafety profile is carefully investigated. In addition, photothermal conversion is characterized for both photoacoustic imaging and photothermal treatment of cancers. Upon radiolabeling, the performance of the resulting particles for SPECT/CT imaging in vivo is also carried out. Additionally, different combinations of treatments are applied for evaluating the performance of the as-prepared Bi_2S_3 NPs in photothermal- and radiotherapy of tumors. Due to the remarkable photothermal conversion efficiency and large X-ray attenuation coefficient, the implanted tumors are completely eradicated through combined therapies, which highlights the potential of BSA-capped Bi_2S_3 NPs as a novel multifunctional nanotheranostic agent.

Dr. Y. Wang, Dr. J. F. Zeng, Prof. Z. Li, Prof. Z. F. Chai
Center for Molecular Imaging and Nuclear Medicine
School for Radiological and Interdisciplinary Sciences (RAD-X)
Soochow University
Collaborative Innovation Center of Radiation Medicine of Jiangsu Higher Education Institutions
Suzhou 215123, P.R. China
E-mail: zhenli@suda.edu.cn

Y. Y. Wu, Y. J. Liu, J. Shen, L. Lv, L. B. Li
The Second Affiliated Hospital of Soochow University
Suzhou 215004, P.R. China

L. C. Yang, Dr. Y. Y. Wang, Prof. L. W. Zhang
School for Radiological and Interdisciplinary Sciences (RAD-X)
Soochow University
Suzhou 215123, P.R. China
E-mail: zhangls@suda.edu.cn

Prof. M. Y. Gao
Institute of Chemistry
Chinese Academy of Sciences
Beijing 100190, P.R. China
E-mail: gaomy@iccas.ac.cn

DOI: 10.1002/adfm.201601341

1. Introduction

Nanotheranostic agents integrated with complementary multiple diagnostic and therapeutic functions have attracted considerable interest in the field of nanomedicine.[1] Ideally, nanotheranostic agents are easily produced under aqueous conditions and act as an omnipotent nanoplatform for targeting detection and treatment of diseases,[2] with the assistance of external stimuli such as magnetism, light, and X-ray. Hitherto, many stimulus-responsive nanoplatforms have been created based on magnetism nanoparticles (NPs),[3] gold nanostructures,[4] carbon nanomaterials,[5] polymeric nanostructures,[6] and transition metal dichalcogenide (i.e., WS_2, MoS_2, CuS) nanostructures.[7] Among the different nanoplatforms, X-ray responsive nanostructures for computed tomography (CT) imaging and radiotherapy (RT) have become increasingly popular,[8] because they not only serve as the contrast agent for visualizing a 3D reconstruction of the tissues of interest with high spatial resolution,[9] but also act as nanosensitizers for improving the efficacy of RT through selectively inducing oxidative stress and/or breaking up the DNA of the tumor cells with no depth restriction, and meanwhile largely reducing the damage to normal tissues.[10]

In addition to X-ray responsive nanotheranostic agents, near-infrared (NIR) light responsive theranostic agents for photoacoustic (PA) imaging and photothermal therapy (PTT) have also attracted considerable interest due to the satisfying penetration depth of NIR light.[11] PA imaging as a novel imaging technology, based on the thermoelastic expansion of tissues caused by a heat mediator responsive to NIR light, exhibits high sensitivity and penetration depth up to 7 cm.[12] It should be noted that each imaging modality or therapeutic technology has its intrinsic advantages and disadvantages. For example, PA imaging suffers from obscure anatomical information in spite of high sensitivity, while PTT fails to eradicate deeply located tumors owing to dramatic depth-dependent intensity decline of incident light.[13] Therefore, it is highly desirable to

integrate the above complimentary theranostic functions for overcoming their limitations. For instance, by assembling different types of functional materials such as ultrasmall CuS NPs on silica-coated rare earth upconversion particles or Pt shell on iron oxide nanorods, imaging capacity and RT/PTT were synergistically combined.[14] Nonetheless, the simple assembly of different inorganic components will inevitably increase the overall size of the nanotheranostic agents, and consequently facilitate their uptake by reticuloendothelial system and reduce their accumulation in the disease site.[15] In this context, constructing ultrasmall and single-component nanoagents with integrated imaging and therapeutic functions is more practically meaningful but challenging.

Due to the narrow direct bandgap (≈1.3 eV), bismuth sulfide exhibits strong NIR absorbance that makes Bi_2S_3 NPs potentially useful in PTT and PA imaging.[16] In addition, Bi_2S_3 NPs were exploited as a CT contrast agent owing to the large X-ray attenuation coefficient of bismuth element.[17] More importantly, they were also extensively investigated for potential applications in RT due to the remarkable radiotherapeutic enhancement effect under irradiation of X-rays.[18] However, the currently available Bi_2S_3 NPs require rigorous synthetic conditions, or postsynthetic surface modification, which are laborious. A facile aqueous synthesis under ambient conditions is essentially required for the practical biomedical applications.[2c,19] Nonetheless, bismuth (III) cations as strong Lewis acid are readily hydrolyzed leading to the formation of bismuth hydroxide,[20] which makes it extremely difficult to achieving pure, ultrasmall, and stable Bi_2S_3 NPs in aqueous media.

Herein, we report a novel bovine serum albumin (BSA)-mediated biomineralization approach that is highly reproducible for achieving biocompatible Bi_2S_3 NPs. The synthesis is featured by two steps: (1) preacidic conditions for facilitating the coordination of Bi^{3+} ions with BSA and preventing the former from hydrolysis, (2) pH-mediated formation of Bi_2S_3 NPs upon a quick adjustment of the reaction pH up to 12, as shown in **Scheme 1**A. The resulting Bi_2S_3 NPs were characterized by ultrasmall size and excellent colloidal stability. In addition, they exhibited low in vivo toxicity and long circulation time, which are highly desirable for theranostic applications. More importantly, the as-prepared Bi_2S_3 NPs exhibited remarkable NIR-responsive photothermal effects and X-ray triggering sensitization effects which can potentially be applied for tumor ablation through irradiation (Scheme 1B). To the best of our knowledge, such ultrasmall and stable Bi_2S_3 NPs synthesized via aqueous synthetic route for simultaneous PA/SPECT/CT imaging, PTT, and RT treatment applications were not reported before.

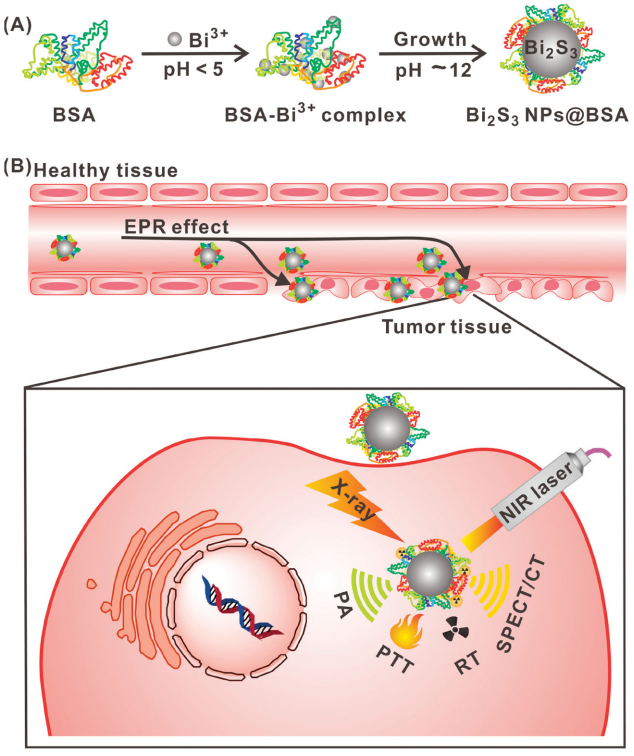

Scheme 1. Schematic illustration of A) BSA-stabilized Bi_2S_3 NPs synthesized through a pH-mediated biomineralization approach, and B) multiple theranostic functions of Bi_2S_3 NPs for PA/CT imaging, SPECT imaging upon radiolabelling, and PTT/RT therapies.

2. Results and Discussion

2.1. Synthesis and Characterization of Bi_2S_3 NPs

In the current synthetic approach, BSA not only served as a stabilizer but also as a sulfur precursor for forming ultrasmall Bi_2S_3 NPs. In addition, its multifunctional groups also provided versatile options for the following surface biofunctionalization.[21] In general, the formation of Bi_2S_3 NPs includes the following procedures, i.e., (i) incubation of BSA with $Bi(NO_3)_3$ to allow BSA to bind with Bi^{3+} ions through its functional groups (e.g., –SH, $–NH_2$, –COOH) for forming BSA-Bi^{3+} complexes in the acid environment (Figure S1, Supporting Information), and (ii) the BSA-Bi^{3+} complexes undergo degradation processes upon alkaline treatment to produce Bi_2S_3 NPs. The latter processes were clearly evidenced by a remarkable color variation from colorless to dark black. It is well-known that BSA can be denatured to release numerous residues (e.g., 35 cysteine residues) under strong basic conditions,[21a,22] and cysteine is an excellent sulfur source for forming metal sulfide NPs.[23] Under strong basic conditions (pH ≈ 12), most thiol groups of cysteine molecules are deprotonated due to the *pKa* of 9.6,[24] which apparently enhances the stabilization effect of BSA for the resulting Bi_2S_3 NPs. Therefore, the solution pH played a crucial role in forming BSA-stabilized Bi_2S_3 NPs (Figure S2, Supporting Information). Most importantly, albumin has been demonstrated to be an ideal drug carrier due to its long blood half time.[25]

The as-prepared Bi_2S_3 NPs are fairly monodispersed with a mean diameter of 6.1 ± 0.9 nm determined with transmission electron microscope (TEM) (**Figure 1**A,B). The small particle size can be attributed to the strong multichelating effects of the BSA ligand. The crystalline structure was identified through the lattice fringes of a single Bi_2S_3 particle shown in the inset of Figure 1A. The interplanar *d*-spacing was determined to be 0.31 nm, well in consistence with (211) lattice plane of monoclinic Bi_2S_3 phase. Although the X-ray diffraction peaks are

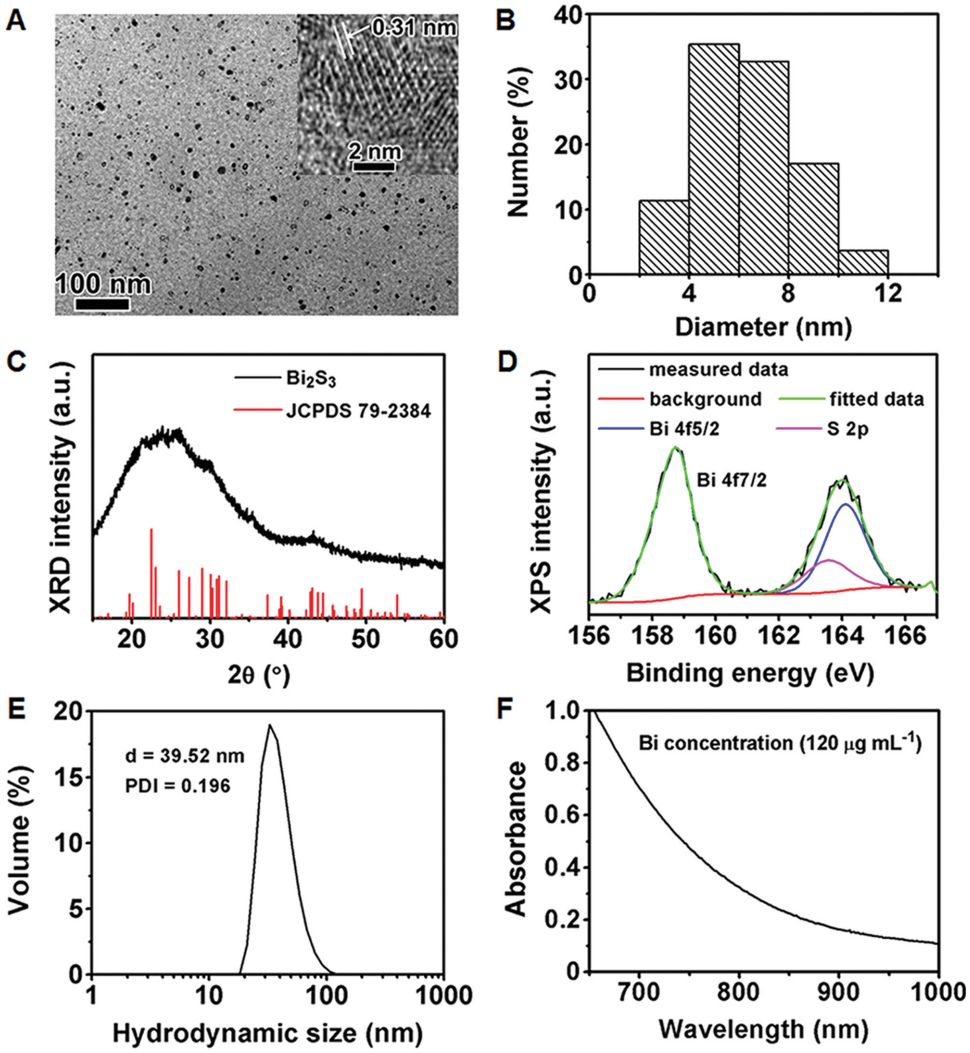

Figure 1. A) TEM image, B) size distribution profile, C) XRD pattern, D) XPS spectrum overlaid with fitting curves for Bi 4f and S 2p, E) hydrodynamic size profile, and F) absorption spectrum of BSA-stabilized Bi_2S_3 NPs (inset: HRTEM image of single Bi_2S_3 NPs).

poorly resolved as shown in Figure 1C, the general diffraction pattern still supports the monoclinic structure (JCPDS 79–2384) of the resulting Bi_2S_3 NPs. The X-ray photoelectron spectroscopy (XPS) results revealed that elemental ratio of Bi-to-S is of 0.45:1 which is smaller than the stoichiometric ratio in bulk Bi_2S_3 mainly due to incomplete reaction of cysteine residues of BSA. Because the binding energies at 158.6 and 164.1 eV can be assigned to Bi $3f_{7/2}$ and Bi $3f_{5/2}$ of Bi_2S_3 NPs and no signal of metallic Bi is present, it can be concluded that the current synthetic route led to Bi_2S_3 NPs.[17c] Regarding the signal at around 163.5 eV, it can be attributed to S 2p from both Bi_2S_3 NPs and the surface BSA (Figure 1D). Fourier transform infrared (FTIR) spectroscopy was also adopted to analyze the resulting NPs. In comparison with BSA denatured under comparable basic conditions, BSA-capped NPs presented a decreased –SH signal intensity at ≈2500 cm^{-1},[23c] suggesting that part of the S content in BSA was converted into Bi_2S_3 NPs (Figure S3, Supporting Information). Since BSA molecules remained anchoring on the particle surface, the resulting NPs were water-dispersible. The dynamic light scattering (DLS) measurements, shown in Figure 1E, reveal that the hydrodynamic size of the resulting NPs is of 39.52 nm. More importantly, they also present excellent colloidal stability (Figure S4, Supporting Information), which is very important for their biomedical applications.[26]

A UV–vis–NIR absorption spectrum of the Bi_2S_3 NPs exhibited a broad absorption extending to the NIR region owing to the narrow bandgap of Bi_2S_3 (Figure 1F), which makes the Bi_2S_3 NPs potentially useful for PTT of tumors. To show the photothermal effects, the temperature of a series of solutions containing different concentrations of Bi_2S_3 NPs was carefully measured after irradiation with an 808 nm laser (0.75 W cm^{-2}) for 600 s. As shown in **Figure 2**A, the temperature increment (ΔT) for Bi_2S_3 NP solutions goes linearly against the concentration of the NPs, while the temperature variation for pure water receiving the same dose of irradiation is negligible. The results given in Figure 2B further reveal that ΔT can be varied from 8.5 to 39.3 °C by simply tuning bismuth concentration from 30 to 240 μg mL^{-1}. These results demonstrate that the Bi_2S_3 NPs can

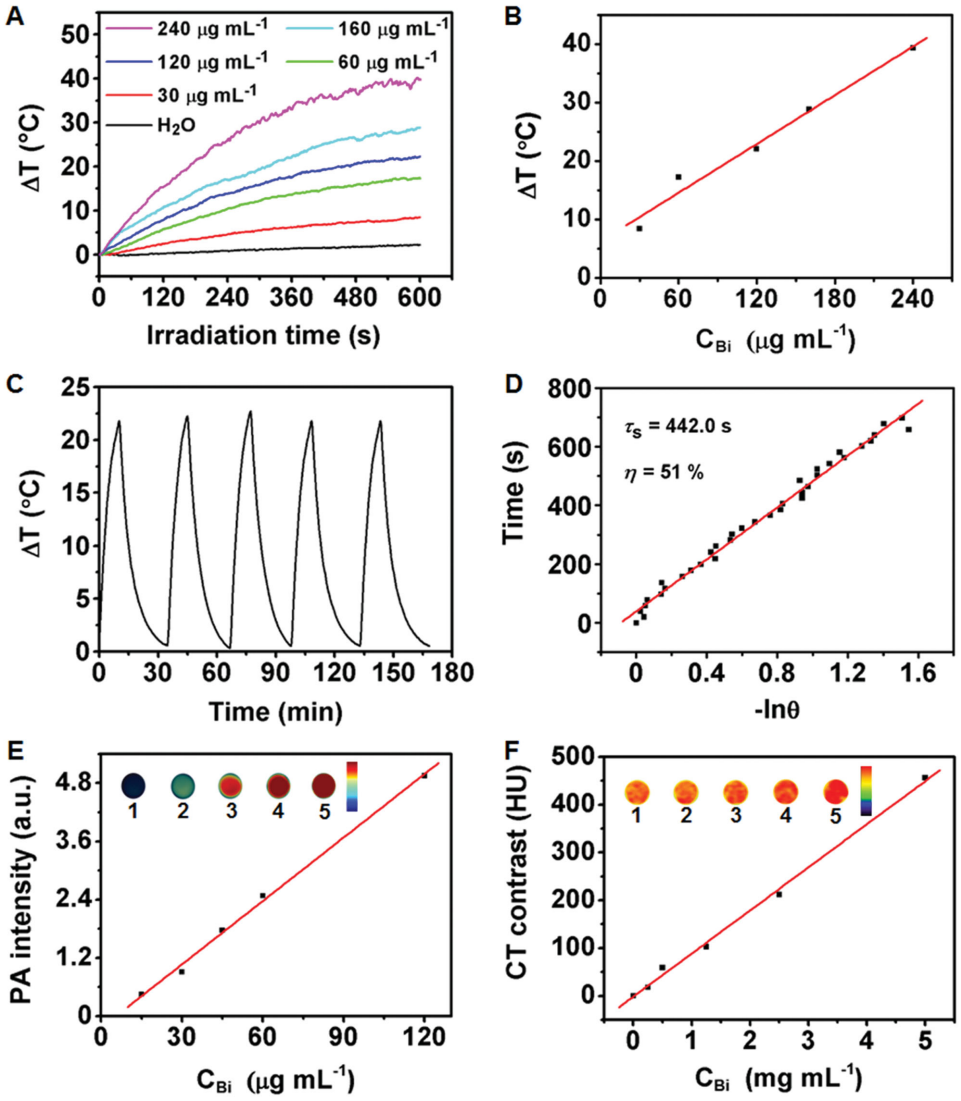

Figure 2. A) Temperature variation curves of 1 mL Bi_2S_3 NPs solutions with different Bi concentrations recorded during 808 nm laser irradiation with a powder density of 0.75 W cm^{-2}; B) Temperature increment of solutions irradiated by 808 nm laser for 600 s against the Bi concentration; C) A temperature variation curve of 1 mL aqueous solution of Bi_2S_3 NPs containing 120 μg Bi recorded during 5 heating/cooling cycles using 808 nm laser as the heating source (10 min natural cooling process was applied following each heating process); D) plot of cooling time (t) versus the negative natural logarithm of the temperature driving force (θ) obtained from the cooling stage as shown in panel (C) for evaluating of the photothermal conversion efficiency (η) with detailed processes shown in the Supporting Information; E) photoacoustic signal intensity of particle solutions as a function of Bi concentration, i.e., (1) 15 μg mL^{-1}, (2) 30 μg mL^{-1}, (3) 45 μg mL^{-1}, (4) 60 μg mL^{-1}, and (5) 120 μg mL^{-1} with the PA images of each solution shown as insets; F) X-ray attenuation of intensity in Hounsfield units (HU) of Bi_2S_3 NPs as a function of Bi concentration, i.e., (1) 0.25 mg mL^{-1}, (2) 0.5 mg mL^{-1}, (3) 1.25 mg mL^{-1}, (4) 2.5 mg mL^{-1}, and (5) 5 mg mL^{-1} with the CT images of each solution shown as insets.

efficiently convert the NIR irradiation (i.e., 808 nm) into heat due to their strong NIR absorbance.

To further show the reliability of the photothermal conversion, ΔT of the solution containing bismuth of 120 μg mL^{-1} was monitored for five successive heating/cooling cycles, during which 10 min irradiation and a natural cooling process were applied. As shown in Figure 2C, the temperature increment achieved during each irradiation cycle remained nearly unchanged, suggesting that Bi_2S_3 NPs are very stable with respect to photothermal conversion. The reliable photothermal conversion is greatly beneficial for quantitatively controlling the local temperature required for therapy. Based on the data shown in Figure 2D, the photothermal conversion efficiency was calculated to be 51% (see the Supporting Information for details). Following the excellent photothermal conversion efficiency, 4T1 cells were chosen for in vitro photothermal ablation tests with the aid of Bi_2S_3 NPs. MTT and live/dead staining studies revealed that Bi_2S_3 NPs can act as a heat mediator for hyperthermia treatment of cancer cells (Figure S5, Supporting Information).

Apart from PTT, the NIR absorption also makes Bi_2S_3 NPs useful for PA imaging. To characterize the imaging performance, the PA signal of a series of Bi_2S_3 NP solutions was

acquired upon excitation at 680 nm and shown in Figure 2E, with the corresponding images shown as inset. The excellent linearity between PA signal and particle concentration is greatly in favor of quantitative imaging studies. Owing to the broad absorption feature, Bi_2S_3 NPs can serve as effective contrast agents over a large spectroscopy region, i.e., from 650 to 980 nm, for PA imaging.

In addition, the large X-ray attenuation coefficient (5.74 $cm^{-2}\cdot kg^{-1}$ at 100 KeV) of Bi element compared with the extensively applied elements such as Au, W, and I (Au: 5.16, W: 4.44, and I: 1.94 $cm^{-2}\cdot kg^{-1}$ at 100 KeV) undoubtedly endows Bi_2S_3 NPs with excellent performance for CT imaging,[27] as shown in Figure 2F. Similar to PA signal, the Hounsfield unit (HU) value also goes linearly against the concentration of the Bi_2S_3 NPs with a slope up to 90.2 HU $L\cdot g^{-1}$, much higher than that of the clinically used iopromide (15.9 HU $L\ g^{-1}$). The excellent CT imaging performance can more directly be visualized through a set of CT images shown as inset of Figure 2F.

2.2. In Vivo Biosafety of Bi_2S_3 NPs

The above results strongly imply that the current Bi_2S_3 NPs can serve as excellent contrast agents for both PA and CT imaging apart from the excellent properties for PTT. Towards these biomedical applications, the possible side effects of the NPs were evaluated through body weight fluctuation, blood chemistry test, and histological evaluation on Sprague Dawley (SD) rats. In detail, SD rats intravenously injected with either 1.0 mL Bi_2S_3 NPs containing 0.5 mg Bi or saline were divided into two groups (n = 5). The body weights of two groups of rats were continually monitored every other day. The results in Figure S6 in the Supporting Information reveal that the body weights of rats injected with Bi_2S_3 NPs decreased in the first 3 d, then gradually increased and became normal on day 10, compared with the control group that received saline injection, suggesting that the Bi_2S_3 NPs exhibited no long-term systemic effects at the given dose.

A complete blood panel analysis was then carried out after the intravenous injection of Bi_2S_3 NPs on the 1st, 3rd, 7th, 14th, and 28th day postinjection. Since any side effects of Bi_2S_3 NPs on the immune system or the potential risks in inducing inflammatory responses will be reflected in hematological factors,[28] the standard hematological and biochemical markers were carefully monitored and compared. The results shown in **Figure 3**, obtained through complete blood count performed at regular intervals, suggest that Bi_2S_3 NPs show no long-term toxicity. For example, there is no significant difference in red blood cells, hemoglobin, hematocrit, or platelets between the control group and the Bi_2S_3 NP treated group. The white blood cell count however slightly increases in the treated group on day 1 and day 3, but recovered to the level of the control group after day 7, indicating a slight immunological stress, as shown in Figure 3C.

Serum biochemical analysis was carried out to show the total protein, albumin, and globulin concentrations in the Bi_2S_3 NP treated rats. A slight increase in total protein on day 7 was observed, primarily due to the increase in globulin, implying a disorder in the immune system or potential inflammation.

Liver injury markers such as alanine aminotransferase (ALT), aspartate aminotransferase (AST), and alkaline phosphatase (ALP) were also evaluated to investigate the risks of Bi_2S_3 NPs. Although there was a slight disorder in ALT before day 7, all values of AST and ALP were rather comparable with those of the control group. In addition, the indicators of kidney injury such as urea and creatinine were massively increased before day 3, but drastically decreased to the normal levels after one week, indicating an acute response of kidney to Bi_2S_3 NPs.

The rats were sacrificed on day 28, major organs such as heart, liver, spleen, lung, and kidney were harvested for weight fluctuation evaluation. The results given in Figure S7 in Supporting Information revealed that there was no big difference in the weights of these organs in comparison with those form the control group. Further hematoxylin and eosin (H&E) staining analysis confirmed that the structural patterns of these organs of the treated group are similar to those of the control group except for the kidney (Figure S8, Supporting Information).

2.3. Pharmacokinetics and Biodistribution of Bi_2S_3 NPs

The biosafety profile of Bi_2S_3 NPs can be attributed to their excellent chemical stability since no release of Bi^{3+} was observed after Bi_2S_3 NPs were incubated in phosphate buffered saline (PBS) containing 10% fetal bovine serum (FBS) over 72 h (Figure S9, Supporting Information). The excellent hemo- and histo-compatibility thus make the BSA-capped Bi_2S_3 NPs potentially useful as a novel theranostic agent. As a long blood circulation time is essentially required for enhancing the accumulation of the NPs in tumors through the enhanced permeability and retention (EPR) effect,[29] the blood circulation behavior was studied by determining the Bi content in blood, drawn from the eye socket of healthy BALB/c mice at different time points after intravenous injection of NPs, with inductively coupled plasma–mass spectroscopy (ICP-MS). By fitting the blood circulation profile shown in **Figure 4**A, the blood half-life was calculated to be around 14.85 h. Such a long blood circulation time can be attributed to the combination of the small hydrodynamic size of BSA coated Bi_2S_3 NPs with the excellent biocompatibility of BSA.

Through the same method, the accumulation of Bi_2S_3 NPs in the tumor and the major organs such as heart, liver, spleen, lung, kidney of 4T1 tumor-bearing BALB/c mice was determined after intravenous administration of Bi_2S_3 NPs (200 µL containing 0.5 mg Bi). The results shown in Figure 4B indicate that the injected Bi_2S_3 NPs are mainly accumulated in the reticuloendothelial organs such as liver and spleen, which is widely observed for nanobiomaterials. Nevertheless, tumor uptake of Bi_2S_3 NPs through the EPR effect is as high as 8.3% ID g^{-1} at 24 h postinjection owing to the excellent blood circulation behavior of Bi_2S_3 NPs.

As aforementioned, the rich functional groups of BSA ligand offer the possibility to further functionalize the Bi_2S_3 NPs. For example, via the strong chelating effect, ^{99m}Tc was successfully used to label the BSA-stabilized Bi_2S_3 NPs,[30] through which the pharmacokinetic behavior of the systemically delivered NPs

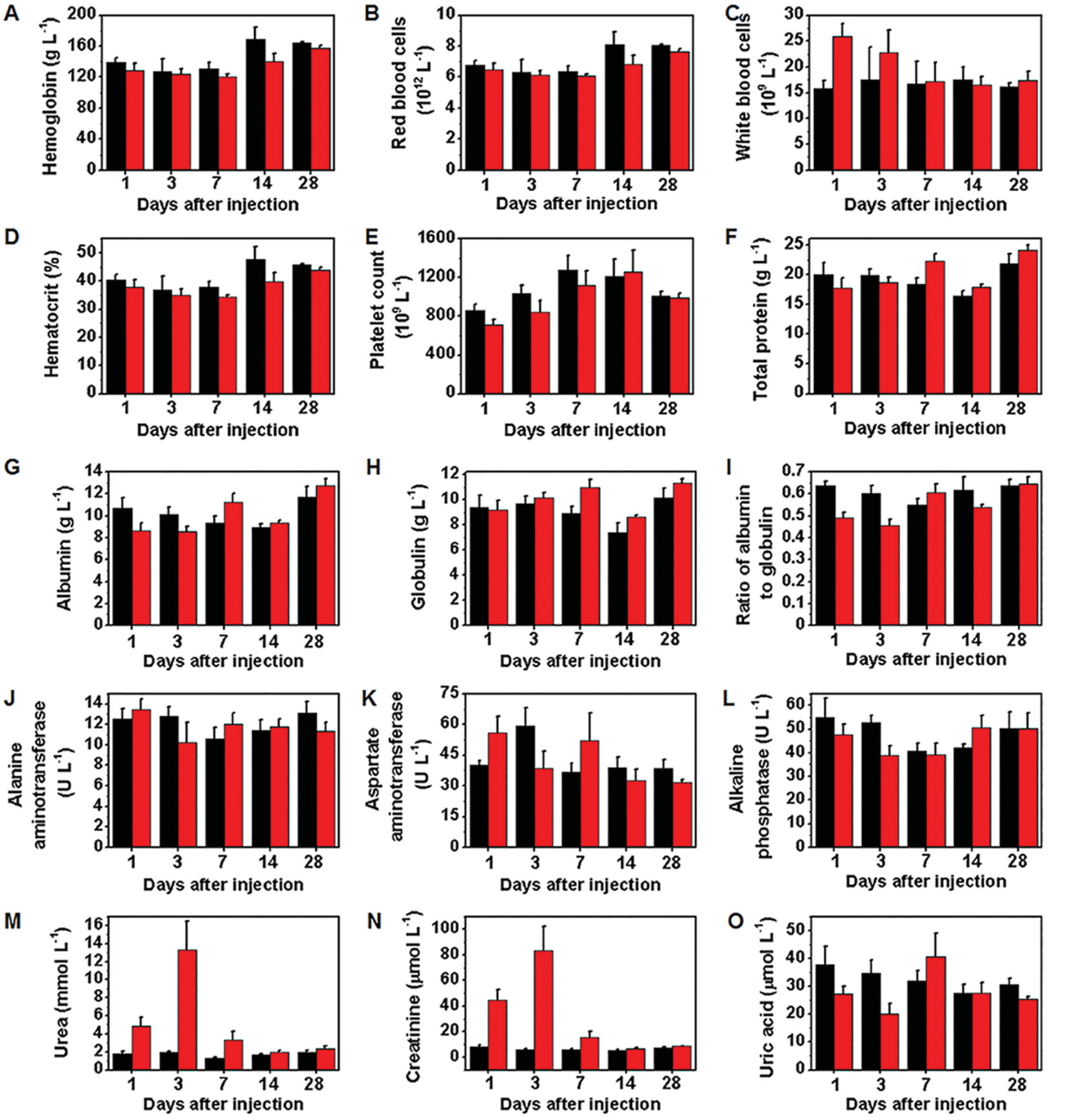

Figure 3. Blood routine and blood biochemical tests on rats intravenously injected with Bi_2S_3 NPs (gray bars) or saline (black bars) as control: A) hemoglobin; B) red blood cell count; C) white blood cell count; D) hematocrit; E) platelet count; F) total protein; G) albumin; H) globulin; I) ratio of albumin to globulin; J) alanine aminotransferase; K) aspartate aminotransferase; L) alkaline phosphatase; M) blood urea nitrogen; N) creatinine; O) uric acid.

can instantly be monitored with single proton emission computed tomography (SPECT). Figure 4C displays the representative SPECT/CT images acquired at different time points, i.e., 1, 2, 6, 12, and 24 h postinjection. Rather in consistence with biodistribution results based on ICP-MS, the SPECT/CT images also reveal a high uptake of Bi_2S_3 NPs in the liver and spleen. More importantly, the SPECT imaging allows the detection of tumor with the aid of the NPs.

2.4. In Vivo PA/CT Imaging of Tumor

The efficient tumor accumulation of Bi_2S_3 NPs is beneficial not only for sensitive detection but also for efficacious therapy of tumors through PTT and RT. For PA imaging of tumors, 200 μL Bi_2S_3 NPs solution containing 0.5 mg Bi were intravenously injected into mice bearing 4T1 tumors. A series of PA images were captured pre-, and 2, 6, and 24 h postinjection are shown

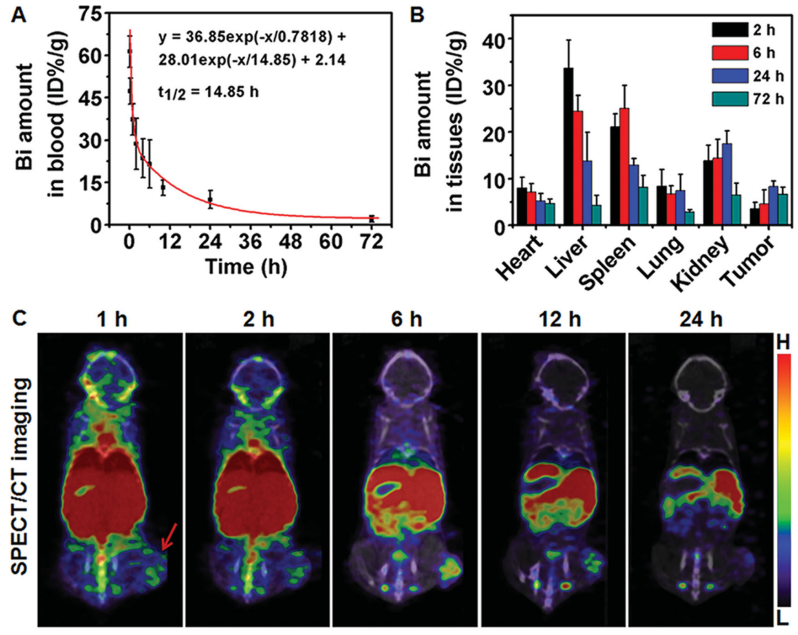

Figure 4. A) Blood circulation profile of Bi_2S_3 NPs fitted with a two-compartment model; B) time-dependent biodistribution of Bi_2S_3 NPs in the mice bearing 4T1 tumors (injection dosage: 200 µL Bi_2S_3 NPs solution containing 0.5 mg Bi); C) SPECT/CT images of a mouse with a 4T1 tumor implanted in the flank region (pointed by red arrow) recorded at different time points after intravenous injection of ^{99m}Tc-labeled Bi_2S_3 NPs (dosage: 200 µL Bi_2S_3 NPs solution containing 0.5 mg Bi, 1 mCi ^{99m}Tc).

2.5. Therapeutic Effects of Bi_2S_3 NPs

Apart from enhancing the imaging contrast, Bi_2S_3 NPs can potentially be used for tumor therapies through PTT and RT sensitization. Based on the above imaging studies that demonstrate the effective tumor accumulation of Bi_2S_3 NPs delivered through tail vein, the following therapeutic studies were carried out. In detail, mice bearing 4T1 tumors intravenously injected with either Bi_2S_3 NPs (200 µL containing 0.5 mg Bi) or saline were divided into six groups (n = 5), i.e., mice injected with saline (group 1, saline), mice injected with Bi_2S_3 NPs (group 2, Bi_2S_3 NPs), mice treated with X-ray irradiation followed by NIR laser after saline injection (group 3, saline + X-ray + NIR), mice treated with NIR laser irradiation after Bi_2S_3 NPs injection (group 4, Bi_2S_3 NPs + NIR), mice treated with X-ray irradiation after Bi_2S_3 NPs injection (group 5, Bi_2S_3 NPs + X-ray), and mice treated with X-ray irradiation followed by NIR laser irradiation after Bi_2S_3 NPs injection (group 6, Bi_2S_3 NPs + X-ray + NIR). Note that all therapeutic irradiations were applied 12 h postinjection of either NPs or

in **Figure 5**A. Rather in consistence with the pharmacokinetics results given in Figure 4, and the signal intensity of tumorous area all the way increases within the inspection time as quantitatively shown in Figure 5C, suggesting that the increased PA signal is mainly induced by Bi_2S_3 NPs. The effective accumulation of Bi_2S_3 NPs can better be seen through the reconstructed 3D images given in Figure S10 in Supporting Information.

Regarding the CT contrast enhancing performance of Bi_2S_3 NPs, an intratumoral injection of 50 µL of Bi_2S_3 NP solution containing 0.125 mg Bi well increased the tumor HU value from 43 to 470 (Figure S11, Supporting Information). However, the CT contrast enhancing effect is largely determined by the effective tumor accumulation of the Bi_2S_3 NPs delivered intravenously. Therefore, the injection dose was evaluated and a series of CT images of a tumor-bearing mouse were captured after intravenous injection of 200 µL of Bi_2S_3 NPs containing 1 mg Bi. The results shown in Figure 5B suggest that the signal of tumor site is slightly increased, which is quantitatively depicted in Figure 5D. The temporal signal evolution tendency rather resembles that of PA signals and the tumor HU value is increased from 20.2 to 58.1 24 h postinjection.

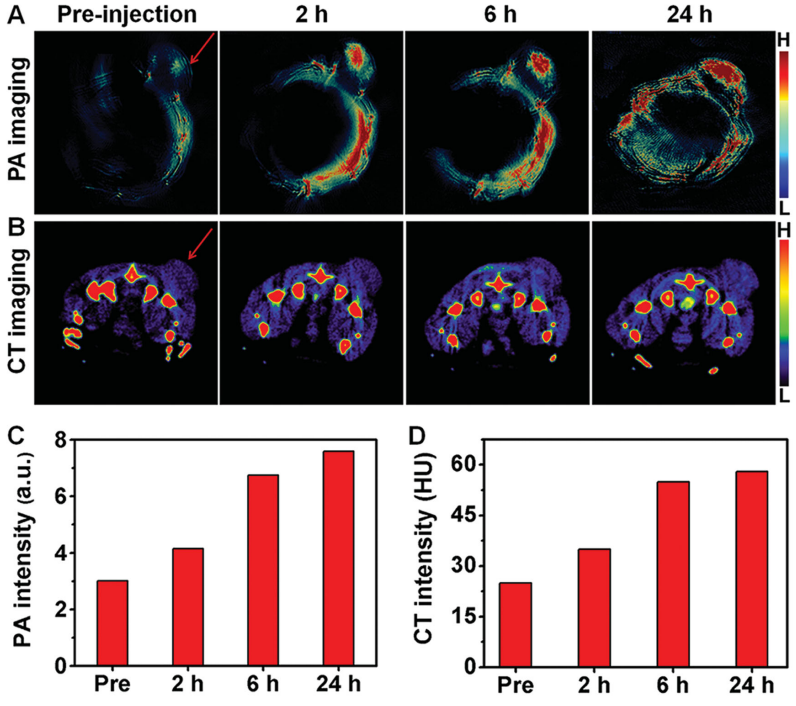

Figure 5. A) In vivo PA images and C) PA signal intensities of the tumorous area recorded pre-, and 2, 6, and 24 h after intravenous injection of Bi_2S_3 NPs into mice bearing 4T1 tumors (dosage: 200 µL Bi_2S_3 NPs solution containing 0.5 mg Bi). B) In vivo CT images and D) the signal intensities of the tumorous area of another group of tumor-bearing mice recorded pre-, and 2, 6, and 24 h after intravenous injection of Bi_2S_3 NPs (dosage: 200 µL of Bi_2S_3 NPs containing 1 mg Bi). The tumor site is pointed by red arrows.

FULL PAPER

saline. The X-ray irradiation with a dose of 4 Gy was applied for five minutes and an 808 nm laser with a power density of 0.75 W cm^{-2} was applied for 5 min after the X-ray irradiation, if they were combined.

During the NIR laser irradiation, an infrared camera was used to capture the full-body thermal images for monitoring the temperature variation of the irradiated area. As shown in **Figure 6**A, the surface temperature of tumorous site is drastically increased for groups receiving Bi_2S_3 NPs, i.e., group 4 and group 6, contrasting to those receiving saline. 5 min of irradiation was enough to increase the temperature of the tumorous site up to ≈50 °C as shown in Figure 6B. The tumor growth curves and the representative photographs of mice chosen from each group are shown in Figure 6C and Figure S11 in Supporting Information, respectively. The results reveal that Bi_2S_3 NPs do not show any tumor treatment effect (group 2). But with the aid of X-ray (group 5), the treatment effect become obvious and comparable with group 2 that received combined RT and PTT treatments in the absence of Bi_2S_3 NPs. The efficacy of PTT achieved with the aid of Bi_2S_3 NPs is apparently

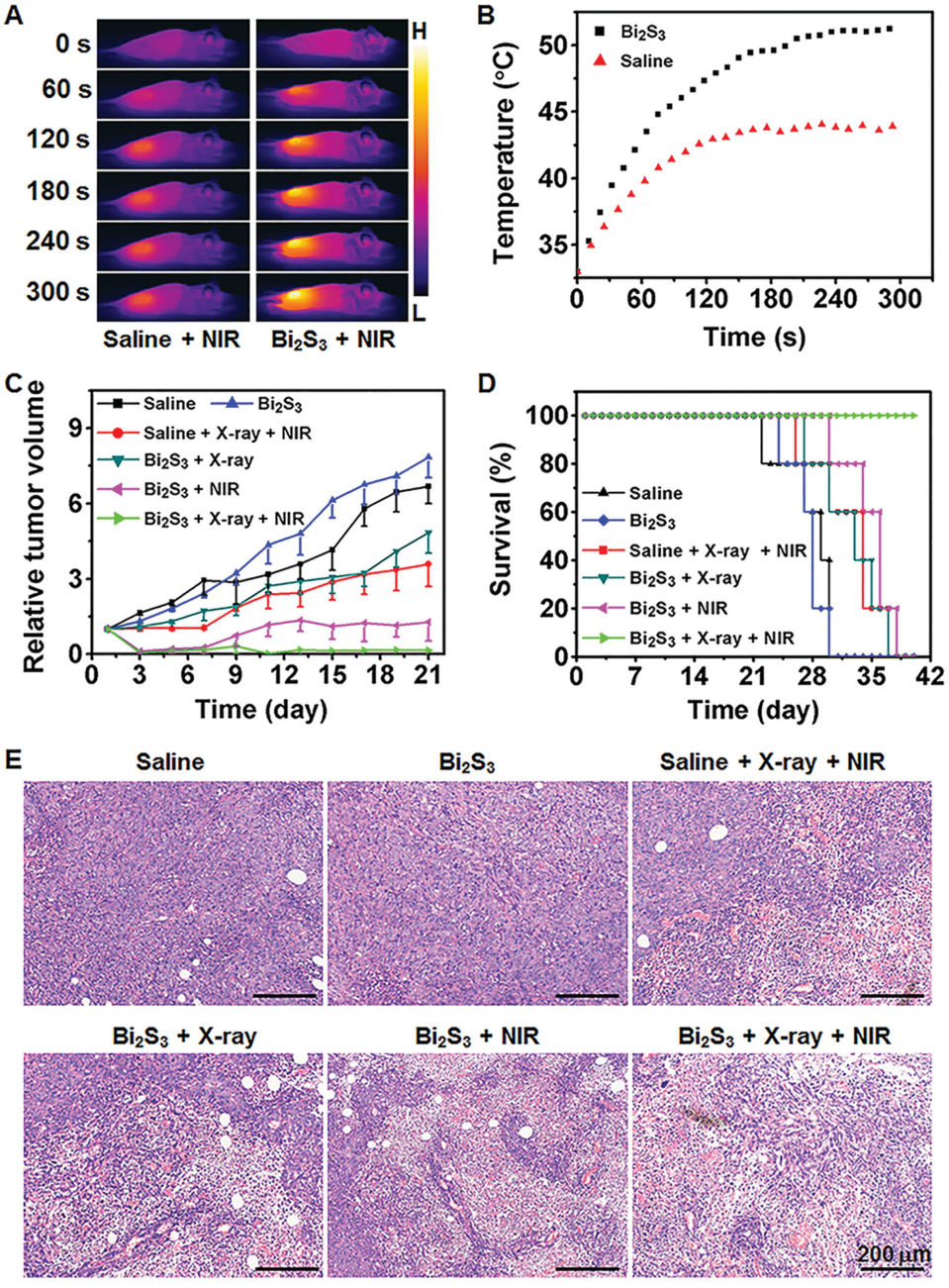

Figure 6. A) Infrared thermal images and B) tumor surface temperature profiles of tumor-bearing mice recorded during the laser irradiation after intravenous injection of saline or Bi_2S_3 NPs (200 μL Bi_2S_3 NPs solution containing 0.5 mg Bi); C) tumor growth inhibition profiles and D) survival rates of six groups of mice ($n = 5$) as a function of time post-treatments; E) H&E staining of tumor tissues harvested from the different groups of mice.

quite substantial (group 4), and can further be improved if RT is applied (group 6), which well manifests the outstanding therapeutic effects of the Bi_2S_3 NPs for combined RT/PTT treatment of tumors. The synergistic effect may be attributed to the facts that Bi_2S_3 NPs-mediated RT can easily killed the radiosensitive cells deep inside the body, while PPT can damage the radio-resistant hypoxic cells and the superficial cancer cells.[8e] Moreover, the tumors were thoroughly eradicated for group 6 within 15 d with no recurrence being observed in 30 d after the treatment, as shown in Figure S12 in Supporting Information.

To fully assess the benefit of Bi_2S_3 NP-directed tumor eradication, the survival rates of mice in different groups were continually monitored. As shown in Figure 6D, all mice from group 1 and group 2 were dead around 30 d post-treatment, owing to the malignant proliferation and abnormal lung metastasis of the tumor. The life span of mice from group 3 and group 4 was obviously prolonged, but all mice were dead after 37 d post-treatment. Although the life span of mice treated by PTT with the aid of Bi_2S_3 NPs was slight increased, but the survival rate went down to zero again 38 d after the treatment. Only mice from group 6 that received combined treatment of PTT and RT after intravenous injection of the Bi_2S_3 NPs NIR presented 100% survival rate over 40 d post-treatment.

The histological changes in the tumor tissues collected on day 1 after the treatment were collected and examined by H&E staining. Serious tumor damage and irregular widening of intercellular spaces can be observed from mice in group 4 and group 5, as shown in Figure 6E, while more severe more damage is presented in mice from group 6, which is rather consistence with the inhibition of tumor growth observed during the earlier stage of different treatments, further demonstrating the synergist effect of Bi_2S_3 NPs for combined PTT/RT therapy of tumors. According to literature,[31] pulmonary metastasis of cancers could become a major cause of death, so the lungs of mice were harvested one month after treatment and carefully examined. As revealed by the H&E staining of lung and other tissues shown in Figure S13 in Supporting Information, aggressive lung metastases were found in almost all mice except for those from group 6, which provides a solid histopathological proof on the excellent therapeutic effects of the Bi_2S_3 NPs for combined PTT/RT treatments of cancers.

3. Conclusion

In summary, BSA-stabilized Bi_2S_3 NPs have been synthesized through a facile one-pot approach for SPECT/CT/PA imaging-guided diagnosis and combined PTT/RT of tumors. The in vivo risk of the BSA-capped Bi_2S_3 NPs are carefully evaluated through body-weight fluctuation, blood chemistry test, and histological evaluation on SD rats, which show a satisfying biosafety profile for Bi_2S_3 NPs. Owing to the ultrasmall size and colloidal stability, the resulting BSA-capped Bi_2S_3 NPs present outstanding blood circulation behavior with a blood half-life up to 14.85 h, which is greatly in favor of tumor uptake for the following PA/CT imaging. Although the Bi_2S_3 NPs themselves do not exhibit any therapeutic effect, their excellent photothermal and radiosensitization effects synergistically enable effective eradication of tumors with the survival rate of tumor-bearing mice up to 100% over 40 d after the treatments. All these studies imply that the BSA-capped Bi_2S_3 NPs may hold a great potential in future biomedical application.

Supporting Information

Supporting Information is available from the Wiley Online Library or from the author.

Acknowledgements

Y.W., Y.Y.W., and Y.L. contributed equally to this work. This work was supported by National Natural Science Foundation of China (21505096, 81471657, 81530057, 81527901, 51503139), Postdoctoral Research Program of Jiangsu Province (1401062C and 1402109C), Postdoctoral Science Foundation of China (2014M560442, 2015M571796, and 2015T80575), Natural Science Foundation of the Jiangsu Higher Education Institutions of China (15KJB150025), The Priority Academic Program Development of Jiangsu Higher Education Institutions (PAPD), and Jiangsu Provincial Key Laboratory of Radiation Medicine and Protection. Z.L. acknowledges the support from the program of Jiangsu Specially Appointed Professorship and Young Thousand Talented Program in China. The authors would like to thank Dr. Tania Silver for critical reading of the manuscript.

Received: March 16, 2016
Revised: April 18, 2016
Published online: May 23, 2016

[1] a) S. Kunjachan, J. Ehling, G. Storm, F. Kiessling, T. Lammers, *Chem. Rev.* **2015**, *115*, 10907; b) G. Chen, I. Roy, C. Yang, P. N. Prasad, *Chem. Rev.* **2016**, *116*, 2826.

[2] a) C. Li, *Nat. Mater.* **2014**, *13*, 110; b) E. K. Lim, T. Kim, S. Paik, S. Haam, Y. M. Huh, K. Lee, *Chem. Rev.* **2015**, *115*, 327; c) Y. Min, J. M. Caster, M. J. Eblan, A. Z. Wang, *Chem. Rev.* **2015**, *115*, 11147.

[3] a) N. Lee, D. Yoo, D. Ling, M. H. Cho, T. Hyeon, J. Cheon, *Chem. Rev.* **2015**, *115*, 10637; b) J. Yu, C. Yang, J. Li, Y. Ding, L. Zhang, M. Z. Yousaf, J. Lin, R. Pang, L. Wei, L. Xu, F. Sheng, C. Li, G. Li, L. Zhao, Y. Hou, *Adv. Mater.* **2014**, *26*, 4114; c) J. Yu, Y. Ju, L. Zhao, X. Chu, W. Yang, Y. Tian, F. Sheng, J. Lin, F. Liu, Y. Dong, Y. Hou, *ACS Nano* **2016**, *10*, 159; d) D. Ho, X. Sun, S. Sun, *Acc. Chem. Res.* **2011**, *44*, 875.

[4] a) X. Yang, M. Yang, B. Pang, M. Vara, Y. Xia, *Chem. Rev.* **2015**, *115*, 10410; b) M. Chen, S. Tang, Z. Guo, X. Wang, S. Mo, X. Huang, G. Liu, N. Zheng, *Adv. Mater.* **2014**, *26*, 8210.

[5] G. Hong, S. Diao, A. L. Antaris, H. Dai, *Chem. Rev.* **2015**, *115*, 10816.

[6] a) M. Elsabahy, G. S. Heo, S.-M. Lim, G. Sun, K. L. Wooley, *Chem. Rev.* **2015**, *115*, 10967; b) Y. Liu, K. Ai, J. Liu, M. Deng, Y. He, L. Lu, *Adv. Mater.* **2013**, *25*, 1353; c) Q. Fan, K. Cheng, X. Hu, X. Ma, R. Zhang, M. Yang, X. Lu, L. Xing, W. Huang, S. S. Gambhir, Z. Cheng, *J. Am. Chem. Soc.* **2014**, *136*, 15185.

[7] a) Y. Chen, C. Tan, H. Zhang, L. Wang, *Chem. Soc. Rev.* **2015**, *44*, 2681; b) L. Cheng, J. Liu, X. Gu, H. Gong, X. Shi, T. Liu, C. Wang, X. Wang, G. Liu, H. Xing, W. Bu, B. Sun, Z. Liu, *Adv. Mater.* **2014**, *26*, 1886; c) T. Liu, C. Wang, X. Gu, H. Gong, L. Cheng, X. Shi, L. Feng, B. Sun, Z. Liu, *Adv. Mater.* **2014**, *26*, 3433; d) M. Zhou, R. Zhang, M. Huang, W. Lu, S. Song, M. P. Melancon, M. Tian, D. Liang, C. Li, *J. Am. Chem. Soc.* **2010**, *132*, 15351; e) T. Liu, S. Shi, C. Liang, S. Shen, L. Cheng, C. Wang, X. Song, S. Goel, T. E. Barnhart, W. Cai, Z. Liu, *ACS Nano* **2015**, *9*, 950.

[8] a) Y. Dou, Y. Guo, X. Li, X. Li, S. Wang, L. Wang, G. Lv, X. Zhang, H. Wang, X. Gong, J. Chang, *ACS Nano* **2016**, *10*, 2536; b) X.-D. Zhang, J. Chen, Y. Min, G. B. Park, X. Shen, S.-S. Song, Y.-M. Sun, H. Wang, W. Long, J. Xie, K. Gao, L. Zhang, S. Fan, F. Fan, U. Jeong, *Adv. Funct. Mater.* **2014**, *24*, 1718; c) H. Xing, X. Zheng, Q. Ren, W. Bu, W. Ge, Q. Xiao, S. Zhang, C. Wei, H. Qu, Z. Wang, Y. Hua, L. Zhou, W. Peng, K. Zhao, J. Shi, *Sci. Rep.* **2013**, *3*, 1751; d) Y. Yong, X. Cheng, T. Bao, M. Zu, L. Yan, W. Yin, C. Ge, D. Wang, Z. Gu, Y. Zhao, *ACS Nano* **2015**, *9*, 12451; e) G. Song, C. Liang, H. Gong, M. Li, X. Zheng, L. Cheng, K. Yang, X. Jiang, Z. Liu, *Adv. Mater.* **2015**, *27*, 6110.

[9] H. Lusic, M. W. Grinstaff, *Chem. Rev.* **2013**, *113*, 1641.

[10] a) P. Prasad, C. R. Gordijo, A. Z. Abbasi, A. Maeda, A. Ip, A. M. Rauth, R. S. DaCosta, X. Y. Wu, *ACS Nano* **2014**, *8*, 3202; b) M. P. Antosh, D. D. Wijesinghe, S. Shrestha, R. Lanou, Y. H. Huang, T. Hasselbacher, D. Fox, N. Neretti, S. Sun, N. Katenka, L. N. Cooper, O. A. Andreev, Y. K. Reshetnyak, *Proc. Natl. Acad. Sci. USA* **2015**, *112*, 5372; c) S. Dufort, A. Bianchi, M. Henry, F. Lux, G. Le Duc, V. Josserand, C. Louis, P. Perriat, Y. Cremillieux, O. Tillement, J.-L. Coll, *Small* **2015**, *11*, 215.

[11] a) L. Cheng, C. Wang, L. Feng, K. Yang, Z. Liu, *Chem. Rev.* **2014**, *114*, 10869; b) K. Ding, L. Jing, C. Liu, Y. Hou, M. Gao, *Biomaterials* **2014**, *35*, 1608; c) Y. Wang, C. Dai, X. P. Yan, *Chem. Commun.* **2014**, *50*, 14341; d) Y. Wang, J. T. Chen, X. P. Yan, *Anal. Chem.* **2013**, *85*, 2529.

[12] a) C. Kim, C. Favazza, L. V. Wang, *Chem. Rev.* **2010**, *110*, 2756; b) J. F. Lovell, C. S. Jin, E. Huynh, H. Jin, C. Kim, J. L. Rubinstein, W. C. Chan, W. Cao, L. V. Wang, G. Zheng, *Nat. Mater.* **2011**, *10*, 324; c) K. Pu, A. J. Shuhendler, J. V. Jokerst, J. Mei, S. S. Gambhir, Z. Bao, J. Rao, *Nat. Nanotechnol.* **2014**, *9*, 233.

[13] a) Z. Zhang, J. Wang, C. Chen, *Adv. Mater.* **2013**, *25*, 3869; b) K. F. Chu, D. E. Dupuy, *Nat. Rev. Cancer* **2014**, *14*, 199.

[14] a) Q. Xiao, X. Zheng, W. Bu, W. Ge, S. Zhang, F. Chen, H. Xing, Q. Ren, W. Fan, K. Zhao, Y. Hua, J. Shi, *J. Am. Chem. Soc.* **2013**, *135*, 13041; b) Y. Deng, E. Li, X. Cheng, J. Zhu, S. Lu, C. Ge, H. Gu, Y. Pan, *Nanoscale* **2016**, *8*, 3895.

[15] a) J. Liu, M. Yu, C. Zhou, S. Yang, X. Ning, J. Zheng, *J. Am. Chem. Soc.* **2013**, *135*, 4978; b) J. Liu, M. Yu, X. Ning, C. Zhou, S. Yang, J. Zheng, *Angew. Chem., Int. Ed.* **2013**, *52*, 12572; c) M. Yu, J. Zheng, *ACS Nano* **2015**, *9*, 6655; d) Z. Li, Q. Sun, Y. Zhu, B. Tan, Z. P. Xu, S. X. Dou, *J. Mater. Chem. B* **2014**, *2*, 2793; e) S. Kunjachan, F. Gremse, B. Theek, P. Koczera, R. Pola, M. Pechar, T. Etrych, K. Ulbrich, G. Storm, F. Kiessling, T. Lammers, *ACS Nano* **2013**, *7*, 252; f) R. Kumar, I. Roy, T. Y. Ohulchanskky, L. A. Vathy, E. J. Bergey, M. Sajjad, P. N. Prasad, *ACS Nano* **2010**, *4*, 699.

[16] a) J. W. Thomson, G. Lawson, P. O'Brien, R. Klenkler, M. G. Helander, S. Petrov, Z.-H. Lu, N. P. Kherani, A. Adronov, G. Ozin, *Adv. Mater.* **2010**, *22*, 4395; b) J. Liu, X. Zheng, L. Yan, L. Zhou, G. Tian, W. Yin, L. Wang, Y. Liu, Z. Hu, Z. Gu, C. Chen, Y. Zhao, *ACS Nano* **2015**, *9*, 696.

[17] a) O. Rabin, J. Manuel Perez, J. Grimm, G. Wojtkiewicz, R. Weissleder, *Nat. Mater.* **2006**, *5*, 118; b) D. Pan, E. Roessl, J. P. Schlomka, S. D. Caruthers, A. Senpan, M. J. Scott, J. S. Allen, H. Zhang, G. Hu, P. J. Gaffney, E. T. Choi, V. Rasche, S. A. Wickline, R. Proksa, G. M. Lanza, *Angew. Chem., Int. Ed.* **2010**, *49*, 9635; c) K. Ai, Y. Liu, J. Liu, Q. Yuan, Y. He, L. Lu, *Adv. Mater.* **2011**, *23*, 4886; d) J. M. Kinsella, R. E. Jimenez, P. P. Karmali, A. M. Rush, V. R. Kotamraju, N. C. Gianneschi, E. Ruoslahti, D. Stupack, M. J. Sailor, *Angew. Chem., Int. Ed.* **2011**, *50*, 12308; e) A. L. Brown, P. C. Naha, V. Benavides-Montes, H. I. Litt, A. M. Goforth, D. P. Cormode, *Chem. Mater.* **2014**, *26*, 2266.

[18] a) M.-H. Yao, M. Ma, Y. Chen, X.-Q. Jia, G. Xu, H.-X. Xu, H.-R. Chen, R. Wu, *Biomaterials* **2014**, *35*, 8197; b) S. Wang, X. Li, Y. Chen, X. Cai, H. Yao, W. Gao, Y. Zheng, X. An, J. Shi, H. Chen, *Adv. Mater.* **2015**, *27*, 2775; c) M. Ma, Y. Huang, H. Chen, X. Jia, S. Wang, Z. Wang, J. Shi, *Biomaterials* **2015**, *37*, 447.

[19] a) Z. Cheng, A. Al Zaki, J. Z. Hui, V. R. Muzykantov, A. Tsourkas, *Science* **2012**, *338*, 903; b) S. E. Lohse, C. J. Murphy, *J. Am. Chem. Soc.* **2012**, *134*, 15607; c) R. A. Petros, J. M. DeSimone, *Nat. Rev. Drug Discovery* **2010**, *9*, 615.

[20] a) A. L. Brown, A. M. Goforth, *Chem. Mater.* **2012**, *24*, 1599; b) C. Han, Z. Li, G. Q. Lu, S. Xue Dou, *Nano Energy* **2015**, *15*, 193.

[21] a) Y. Wang, X. P. Yan, *Chem. Commun.* **2013**, *49*, 3324; b) Y. Wang, T. Yang, H. Ke, A. Zhu, Y. Wang, J. Wang, J. Shen, G. Liu, C. Chen, Y. Zhao, H. Chen, *Adv. Mater.* **2015**, *27*, 3874; c) Q. Wang, L. Lv, Z. Ling, Y. Wang, Y. Liu, L. Li, G. Liu, L. Shen, J. Yan, Y. Wang, *Anal. Chem.* **2015**, *87*, 4299; d) M. G. Persico, L. Lodola, F. E. Buroni, M. Morandotti, P. Pallavicini, C. Aprile, *J. Labelled Compd. Radiopharm.* **2015**, *58*, 376; e) Y. Wang, L. Lang, P. Huang, Z. Wang, O. Jacobson, D. O. Kiesewetter, I. U. Ali, G. Teng, G. Niu, X. Chen, *Proc. Natl. Acad. Sci. USA* **2015**, *112*, 208.

[22] J. Xie, Y. Zheng, J. Y. Ying, *J. Am. Chem. Soc.* **2009**, *131*, 888.

[23] a) J. Xiang, H. Cao, Q. Wu, S. Zhang, X. Zhang, A. A. R. Watt, *J. Phys. Chem. C* **2008**, *112*, 3580; b) W.-T. Chen, Y.-J. Hsu, *Langmuir* **2010**, *26*, 5918; c) B. Zhang, X. Ye, W. Hou, Y. Zhao, Y. Xie, *J. Phys. Chem. B* **2006**, *110*, 8978.

[24] X. Q. Chen, Z. Li, Y. Bai, Q. Sun, L. Z. Wang, S. X. Dou, *Chem. Eur. J.* **2015**, *21*, 1055.

[25] a) F. Kratz, *J. Controlled Release* **2008**, *132*, 171; b) Z. Sheng, D. Hu, M. Zheng, P. Zhao, H. Liu, D. Gao, P. Gong, G. Gao, P. Zhang, Y. Ma, L. Cai, *ACS Nano* **2014**, *8*, 12310; c) Q. Chen, C. Liang, C. Wang, Z. Liu, *Adv. Mater.* **2015**, *27*, 903; d) S. Bae, K. Ma, T. H. Kim, E. S. Lee, K. T. Oh, E.-S. Park, K. C. Lee, Y. S. Youn, *Biomaterials* **2012**, *33*, 1536; e) Q. Chen, C. Liang, X. Wang, J. He, Y. Li, Z. Liu, *Biomaterials* **2014**, *35*, 9355; f) W. Cao, X. Lu, Z. Cheng, *Curr. Pharm. Des.* **2015**, *21*, 1908.

[26] a) H. S. Choi, W. Liu, F. Liu, K. Nasr, P. Misra, M. G. Bawendi, J. V. Frangioni, *Nat. Nanotechnol.* **2010**, *5*, 42; b) K. Susumu, E. Oh, J. B. Delehanty, J. B. Blanco-Canosa, B. J. Johnson, V. Jain, W. J. T. Hervey, W. R. Algar, K. Boeneman, P. E. Dawson, I. L. Medintz, *J. Am. Chem. Soc.* **2011**, *133*, 9480.

[27] N. Lee, S. H. Choi, T. Hyeon, *Adv. Mater.* **2013**, *25*, 2641.

[28] L. Ye, K. T. Yong, L. Liu, I. Roy, R. Hu, J. Zhu, H. Cai, W. C. Law, J. Liu, K. Wang, J. Liu, Y. Liu, Y. Hu, X. Zhang, M. T. Swihart, P. N. Prasad, *Nat. Nanotechnol.* **2012**, *7*, 453.

[29] a) G. von Maltzahn, J.-H. Park, A. Agrawal, N. K. Bandaru, S. K. Das, M. J. Sailor, S. N. Bhatia, *Cancer Res.* **2009**, *69*, 3892; b) Z. Liu, F. Pu, S. Huang, Q. Yuan, J. Ren, X. Qu, *Biomaterials* **2013**, *34*, 1712; c) A. Maksimenko, F. Dosio, J. Mougin, A. Ferrero, S. Wack, L. H. Reddy, A.-A. Weyn, E. Lepeltier, C. Bourgaux, B. Stella, L. Cattel, P. Couvreur, *Proc. Natl. Acad. Sci. USA* **2014**, *111*, E217; d) H. Maeda, H. Nakamura, J. Fang, *Adv. Drug Delivery Rev.* **2013**, *65*, 71.

[30] a) D. A. Heuveling, G. W. M. Visser, M. Baclayon, W. H. Roos, G. J. L. Wuite, O. S. Hoekstra, C. R. Leemans, R. de Bree, G. A. M. S. van Dongen, *J. Nucl. Med.* **2011**, *52*, 1580; b) V. L. Gates, N. Singh, R. J. Lewandowski, S. Spies, R. Salem, *J. Nucl. Med.* **2015**, *56*, 1157.

[31] a) A. Schroeder, D. A. Heller, M. M. Winslow, J. E. Dahlman, G. W. Pratt, R. Langer, T. Jacks, D. G. Anderson, *Nat. Rev. Cancer* **2012**, *12*, 39; b) X. Yi, K. Yang, C. Liang, X. Zhong, P. Ning, G. Song, D. Wang, C. Ge, C. Chen, Z. Chai, Z. Liu, *Adv. Funct. Mater.* **2015**, *25*, 4689.